Ab Initio Study of the Physical Properties of Cs-Based Double Perovskites Cs_2AX_6 (A = Ge, Mn; X = Cl, I)

A.A. Yahaya[a,b,*], W.A. Yahya[a], A.S. Ahmed[c] and A.A. Sholagberu[a]

[a] *Department of Physics and Materials Science, Kwara State University, Malete, Nigeria*
[b] *Department of Physics, Kebbi State University of Science and Technology, Aliero, Nigeria*
[c] *Department of Chemistry and Industrial Chemistry, Kwara State University, Malete, Nigeria*

Received: 27.10.2023 & Accepted: 13.12.2023

Doi: 10.12693/APhysPolA.145.194 *e-mail: yahyaabubakaraliero@gmail.com

Device applications in magnetic media, spintronics, oxygen membranes, sensors, etc., are some of the uses of ferrite materials. In this work, we have studied the structural, electronic, magnetic, mechanical, and thermoelectric properties of Cs-based double perovskites Cs_2AX_6 (A = Ge, Mn; X = Cl, I), using Quantum Espresso with generalized gradient approximation Perdew–Burke–Ernzerhof and Perdew–Burke–Ernzerhof in solids exchange–correlation functionals. The band structure results show that Cs_2GeCl_6 and Cs_2MnCl_6 are semiconductors with direct band gaps. However, there are bands crossing observed for Cs_2GeI_6 from the conduction band minimum to the valence band maximum, indicating the metallic nature of the material. Moreover, Cs_2MnI_6 has magnetic properties; it exhibits a metallic nature in the spin-up state and a semiconductor nature in the spin-down state, suggesting that it can be used in spintronics applications. The calculated total magnetic moment of Cs_2MnCl_6 is $3.0\mu_B$ (for both Perdew–Burke–Ernzerhof and Perdew–Burke–Ernzerhof in solids), while for Cs_2MnI_6, the calculated total magnetic moments are $3.02\mu_B$ and $3.06\mu_B$, for Perdew–Burke–Ernzerhof and Perdew–Burke–Ernzerhof in solids exchange–correlation functionals, respectively. The results of the mechanical properties calculations show that Cs-based double perovskites Cs_2AX_6 (A = Ge, Mn; X = Cl, I) are mechanically stable. Cauchy's pressure and Poisson's, Frantsevich's, and Pugh's ratios of the studied materials confirm that Cs_2MnCl_6 is brittle, while the remaining studied double perovskite materials are ductile. Electrical conductivity, thermal conductivity, Seebeck coefficients, power factor, and figure of merit are the thermoelectric parameters analyzed in this study. Seebeck coefficients, electrical conductivity, and power factor increase with the rise in temperature, and Cs_2MnX_6 (X = Cl, I) double perovskite materials have higher values of electrical conductivity than Cs_2GeX_6 (X = Cl, I). All the studied materials have positive type conductivity due to their positive Seebeck coefficient values.

topics: double perovskite; doping; magnetic moment; electronic, mechanical, and thermoelectric properties

1. Introduction

The increasing demand for energy has forced scientific societies to seek alternative solutions to traditional energy sources. Non-renewable energy sources are limited in availability, expensive in nature, have a detrimental influence on our environment, and have a variety of other difficulties that have successfully increased the world's urgency to embrace clean, renewable energy. Solar energy is one of the renewable energy sources and is efficient, clean, abundant, and practical; this energy may be absorbed and used via solar panels with high conversion efficiency, stability, and low-cost photovoltaic technology. Lead halide (organic–inorganic) perovskite materials have long carrier diffusion length, high absorption coefficient, higher charge carrier mobility, and appropriate bang gap, and are fabricated by solution-processable techniques, which makes the materials more popular in photovoltaic applications [1–3]. The tunability of perovskites' electronic and optical parameters makes them appealing for energy and microelectronics applications [1, 4, 5]. The limitations in the technical applications of perovskites are due to their finite electrical conduction, structural stabilities, and toxicity [4, 6, 7]. Finding non-toxic lead-based perovskites requires substantial investigation into other non-toxic metals. Because of the structural tunability of perovskites, a double perovskite with the general structural formula A_2BX_6 was discovered, where A and B are tetravalent and octavalent cations, and X can be Cl, Br, or I (anion halides). These cations and anions might be changed selectively to generate a non-toxic, stable, and efficient perovskite. The heightened interest in double

perovskite materials stems from their distinct advantages over conventional perovskites. These advantages include amplified stability [8], customizable properties, unique magnetic and electronic characteristics [9], tailored band structures, and the formation of functional heterostructures [10]. These collective advantages position double perovskites as promising candidates for next-generation materials across various technological applications, owing to their adjustability and heightened stability compared to traditional perovskites.

The significant characteristics, such as flexibility and diversity of the chemical compositional forms of double perovskite materials, established their importance in modern materials research and technology [11–14]. Manganites and cobalties are among the rare-earth (RE) materials currently receiving a lot of attention among the many known double perovskite materials [14, 15]. Structural, optoelectronic, and magnetic interactions in strongly coupled systems are what initially drew attention to these ferrite materials. Such ferrite materials have good applications in sensors, spintronics, magnetic media electrode materials, and so on [14, 16]. These double perovskites, which are RE-based materials, have drawn the most attention among the diverse spectrum of ferrites due to their intriguing structural properties [14, 17]. As previously stated in [14, 17], the magnetic properties of RE-based oxides are heavily influenced by various synthesis procedures and conditions.

Diao et al. [18] used density functional theory (DFT) to perform high-throughput screening of efficient and stable double inorganic halide perovskite materials using the CASTEP and DMol^3 codes. Stability and photoelectric conversion of 42 inorganic double perovskite materials, including Cs_2GeX_6 (X = Cl, Br, I), were reported. Band gap values of 0.323 eV and 0.347 eV were reported for Cs_2GeBr_6, using the CASTEP and DMol^3 codes, respectively, and 2.179 eV and 2.233 eV were also reported for Cs_2GeCl_6, using the CASTEP and DMol^3 codes, respectively. It was discovered that double perovskite that contains caesium (Cs) tends to have the same structural formation, prevalent band structures, and structural stability and possesses good light absorption properties.

Mahmood et al. [19] investigated optical, thermoelectric, and mechanical properties of double perovskites Cs_2GeCl/Br_6 using a full potential linearized augmented plane wave (FP-LAPW) method as implemented in a DFT code, WIEN2k. It was clear that replacing Cl with Br increases the lattice constant from 1.75 (Cl) to 1.85 A (Br). The calculated Poisson's and Pugh's ratios indicated the ductile nature of Cs_2GeCl/Br_6. They calculated the band gap to be 3.42 eV and 2.15 eV for Cs_2GeCl and Cs_2GeBr_6, respectively, making them ideal for optical applications. The ultraviolet area (UV) has a higher intensity than the visible region, with excitonic peaks in both the visible and ultraviolet regions, making it an excellent material for optoelectronic applications that function in UV light. The authors concluded that the examined double perovskites are viable materials for use in sustainable applications based on their optical and thermoelectric properties results.

Cai et al. [20] also investigated the electronic structure and structural stability of A_2BX_6 inorganic halide Perovskite compounds. They employed spin-polarized PBE-GGA and HSE06 exchange–correlation functionals using VASP (Vienna Ab initio Simulation Package). In their study, they found that the impact of cations on A-site is more complicated. When the size of the A-site cation decreases, the predicted band gap in the cubic structure also decreases. Alloying the A and X sites is expected to be effective in adjusting the stability of the structure and in improving the bandgap.

In this work, Cs-based double perovskites Cs_2AX_6 (A = Ge, Mn; X = Cl, I) materials are studied. The structural, electronic, mechanical, and thermoelectric properties of Cs_2GeX_6 (X = Cl, I) and Cs_2MnX_6 (X = Cl, I) double perovskites are investigated for solar cells and spintronics applications. A plane wave basis set of Quantum ESPRESSO (QE) code has been used in the study of the physical properties of the double perovskite materials Cs_2GeX_6 (X = Cl, I). Furthermore, Ge was replaced by Mn to obtain Cs_2MnX_6 (X = Cl, I), and the physical properties were calculated by considering spin polarization. Generalized gradient approximation Perdew–Burke–Ernzerhof (GGA-PBE) and Perdew–Burke–Ernzerhof in solids (PBESol) exchange–correlation functionals have been utilized. This article is organized as follows: computational details are described in Sect. 2, results and discussions in Sect. 3, and the conclusion in Sect. 4.

2. Computational details

Quantum ESPRESSO code (QE) was used for the calculation of structural, magnetic, electronic, mechanical, and thermoelectric properties of Cs-based double perovskite materials Cs_2AX_6 (A = Ge, Mn; X = Cl, I) [21, 22]. To describe interactions between core and valence electrons, the plane wave method was used. Norm-conserving pseudo potentials were utilized to describe electron–ion interactions using GGA in the form of Perdew–Burke–Ernzerhof (GGA-PBE) and of Perdew–Burke–Ernzerhof for solids (GGA-PBESol) [23]. Cut-off energy convergence was set at 120 Ry, while 10^{-5} eV and 10^{-5} eV/Å were used as energy and force convergence thresholds per atom, respectively, and centred $8 \times 8 \times 8$ k-mesh in the Brillouin zone integration was used [24]. Next, k-points of $8 \times 8 \times 8$ were applied in calculating magnetic, structural, electronic, and mechanical properties, while k-points of $12 \times 12 \times 12$ were used to calculate the density

of states. Positions of atoms were totally optimized for all calculations, and structural relaxation was achieved using the Broyden–Fletcher–Goldfarb–Shanno quasi-Newton algorithm [25, 26].

2.1. Mechanical properties

Certain properties of materials become important when forces are applied to the materials, particularly during manufacturing and fabrication. These properties include elastic and mechanical properties [27–29]. It is very important to understand how mechanically stable the atoms of a material and the atom-to-atom bonding are. Elastic constants (C_{11}, C_{12}, C_{44}) for Cs-based double perovskite materials Cs_2AX_6 (A = Ge, Mn; X = Cl, I) were calculated under ambient conditions. A crystal cannot exist in a stable or meta-stable state unless its elastic constants satisfy the generalized mechanical stability criteria [28, 30]. The Born–Huang elastic criteria theorem is given as [27, 31]

$$C_{11} - C_{12} > 0, \tag{1}$$

$$C_{11} - 2C_{12} > 0, \tag{2}$$

$$C_{44} > 0, \tag{3}$$

and

$$C_{11} < B < C_{44}. \tag{4}$$

The bulk modulus (B) was determined using

$$B = \frac{C_{11} + 2C_{12}}{3}. \tag{5}$$

Chung and Buessem [32] harmonized the Voigt–Reuss–Hill approximation (VHR) into a relationship between some isotropic characteristics (bulk modulus, shear modulus, and Young modulus) and the elastic constant defined by Voigt, Reuss, and Hill. This method converts anisotropic elastic constants into isotropic polycrystalline elastic moduli. The following are Voigt's [33] elastic moduli equations

$$B_V = \frac{C_{11} + 2C_{12}}{3}, \tag{6}$$

$$G_V = \frac{C_{11} - C_{12} + 3C_{44}}{5}, \tag{7}$$

where B_V and G_V are the isotropic bulk modulus and shear modulus, respectively. For a cubic structure, Reuss's bulk modulus (B_R) and Voigt's bulk modulus (B_V) are equivalent. Reuss's shear modulus (G_R) is expressed as follows [34]

$$G_R = \frac{5\,(C_{11} - C_{12})\,C_{44}}{4C_{44} + 3\,(C_{11} - C_{12})}. \tag{8}$$

Hill's elastic moduli approximation is the average values of Voigt's and Reuss's elastic moduli, which are

$$B_H = \frac{1}{2}(B_V + B_R), \tag{9}$$

$$G_H = \frac{1}{2}(G_V + G_R). \tag{10}$$

Hill's bulk (G_H) and shear moduli (B_H) are given by (9) and (10), respectively [35].

The values of shear anisotropy (A), Cauchy's pressure (P_C), Young's modulus (Y), Poisson's ratio (ν), Pugh's ratio (R_P), and Frantsevich's ratio (R_F) were calculated using the following equations [36]

$$A = \frac{2C_{44}}{C_{11} - C_{12}}, \tag{11}$$

$$P_C = C_{12} - C_{44}, \tag{12}$$

$$Y = \frac{9BG}{3B + G}, \tag{13}$$

$$v = \frac{3B - 2G}{6B + 2G}, \tag{14}$$

$$R_p = \frac{B}{G}, \tag{15}$$

$$R_f = \frac{G}{B}. \tag{16}$$

2.2. Thermoelectric properties

The thermoelectric (TE) properties of the studied Cs-based double perovskite materials Cs_2AX_6 (A = Ge, Mn; X = Cl, I) were calculated using the BoltzTraP2 package [37] using both GGA (PBE and PBESol) exchange–correlation functionals. Electronic thermal conductivity (κ_e), Seebeck coefficient (S), electrical conductivity (σ), power factor (PF), and figure of merit (ZT) are the thermoelectric properties calculated in this study. The BoltzTraP2 package operates within the framework of DFT, as implemented in the QE code, and a relaxation time constant of ($\tau = 10^{-14}$ s) was used. Figure of merit (ZT) is strongly influenced by the Seebeck coefficient (S) and electronic and thermal conductivity (κ_e), and these thermoelectric parameters depend on the relaxation time constant. All the TE properties are calculated within temperature (T) values in the range of 150–1300 K. Power factor is calculated using [38]

$$PF = S^2\sigma, \tag{17}$$

while the figure of merit (ZT) was computed using [39]

$$ZT = \frac{\sigma S^2}{\kappa_e} T. \tag{18}$$

3. Results and discussion

3.1. Structural properties

Cs-based double perovskite materials Cs_2AX_6 (A = Ge, Mn; X = Cl, I) have space group of $Fm{-}3m$, face-centred cubic (fcc) structure, with

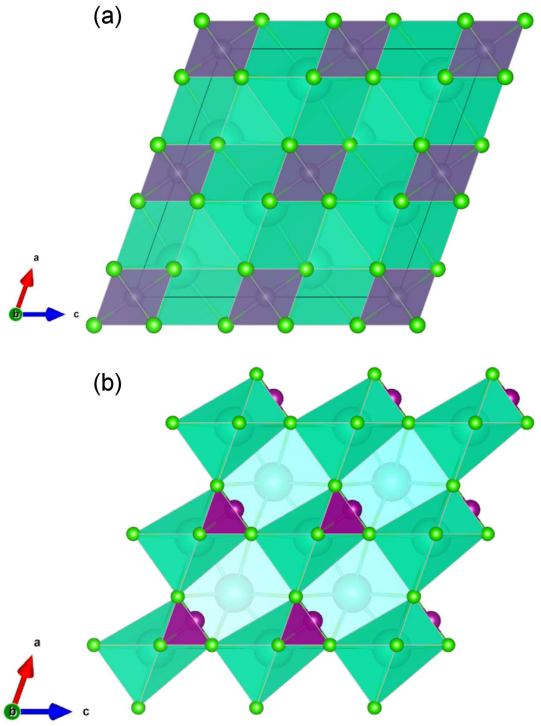

Fig. 1. Polyhedral crystal structure of (a) Cs_2GeCl_6 and (b) Cs_2MnCl_6.

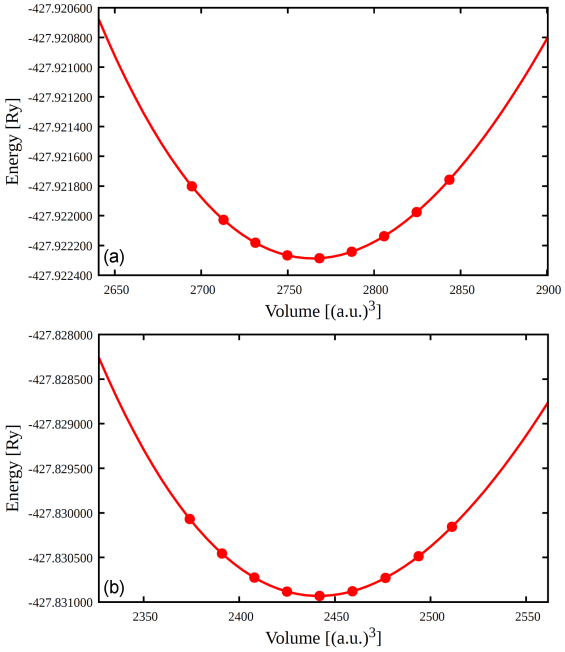

Fig. 2. Cs_2GeCl_6 optimized energy versus volume plots calculated with GGA (a) PBE and (b) PBESol.

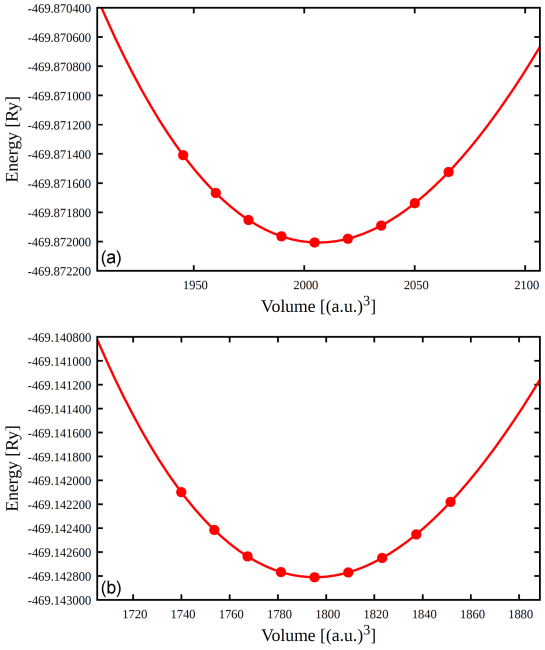

Fig. 3. Cs_2GeI_6 optimized energy versus volume plots calculated with GGA (a) PBE and (b) PBESol.

coordination of Cs_2^+ in 12-fold cubo-octahedral surrounded in 6-fold coordination by each Ge^+ and Mn^+ cation alternating along the planes of [001], [010], and [100], as shown in Fig. 1. In the figure, light teal colour denotes Cs atoms, grey and violet colour denote Ge and Mn atoms, respectively, and lime colour denotes the Cl atoms.

Ground state energy of the atoms is required for the description of any material's quantitative mechanical properties. Atoms in solids can be in their ground state by minimising crystals energy [27]. A plane wave basis set was used in the structural parameters calculation of the studied double perovskite materials. Birch–Murngham's equation of state was used to calculate the system's equilibrium volume by fitting the total energy as a function of volume using GGA-PBE and PBESol exchange–correlation functionals. The graphs of optimized energy against volume in Figs. 2 and 3 obtained with both GGA-PBE and PBESol of the studied Cs-based double perovskite materials indicate the equilibrium volume at which the total energy of the examined double perovskite materials becomes minimum. Excellent electronic structure measurement will be obtained when internal parameters are relaxed by minimising the total energy of the studied Cs-based double perovskite materials.

Lattice constant at equilibrium (a), bulk modulus (B), bulk modulus pressure derivative ($B^{'}$), unit cell volume (V), and enthalpy (given in Ry) calculated using Birch–Murngham's equation of state are shown in Table I. According to the table, Cs_2GeI_6 and Cs_2MnI_6 have higher a [Å], B [GPa], $B^{'}$, and V [Å^3] values. The results show that the values of lattice constant and unit cell volume at equilibrium rise from Cl to I anion due to the increasing atomic size of the anion, i.e., that iodine anion has a higher ionic radius than chlorine anion [40, 41].

3.2. Electronic properties

Electronic properties influence material applications in device engineering. These properties classify the materials in order to reveal the carrier transport mechanism; they also reveal the materials' semiconductor, insulator, semimetal, and metal nature. Band structure and density of states (DOS) of Cs-based double perovskite materials Cs_2AX_6 (A = Ge, Mn; X = Cl, I) were studied using both GGA-PBE and PBESol exchange–correlation functionals to reveal their electronic properties.

3.2.1. Band structure

A turning point in revealing the nature of the material is known as band structure. Band structure can reveal a material's metallic, semiconducting, and insulating properties. According to [42], the band structure is the foundation for solid-state devices (transistors, solar cells, etc.), and the optical behaviour and electrical resistivity of a material can be explained using band structures. Band structures of Cs_2AX_6 (A = Ge, Mn; X = Cl, I) were studied using both GGA-PBE and PBESol. Spin-polarized calculations were carried out for Cs_2MnX_6 (X = Cl, I) due to the presence of a transition metal (Mn). The substitution of chloride with iodide induces alterations in the band structure due to differences in ionic size, electronegativity, and other electronic properties. This modification affects the energies of both the valence and conduction bands, consequently influencing the type of band gap energies or influencing the nature of the material — either insulator, semiconductor, or conductor. Additionally, the choice of transition metals significantly shapes the electronic structure of perovskite materials. For example, manganese and germanium possess distinct electronic configurations and bonding characteristics. The inclusion of these metals alters the band structure, thereby modifying the energies of both the direct and indirect band gaps. The calculated band gaps are given in Table II (see also [18, 19]).

TABLE I

Calculated structural properties of Cs-based double perovskite materials Cs_2AX_6 (A = Ge, Mn; X = Cl, I) with GGA-PBE and PBESol.

Materials		a [Å]	B [GPa]	B'	V [Å^3]
Cs_2GeCl_6	GGA-PBE	19.29	11.33	5.74	2065.35
	GGA-PBESol	20.02	8.76	6.37	1851.58
Cs_2GeI_6	GGA-PBE	22.27	7.47	7.37	2843.58
	GGA-PBESol	21.37	12.50	8.07	2511.16
Cs_2MnCl_6	GGA-PBE	19.86	8.92	6.66	2022.77
	GGA-PBESol	19.11	11.73	6.66	1801.71
Cs_2MnI_6	GGA-PBE	22.08	7.34	6.60	2765.38
	GGA-PBESol	21.15	12.09	7.86	2435.20

TABLE II

Calculated electronic band gaps of Cs-based double perovskite materials Cs_2AX_6 (A = Ge, Mn; X = Cl, I) using GGA-PBE and PBESol.

Material		GGA-PBE [eV]	GGA-PBESol [eV]	Other calc. [eV]
Cs_2GeCl_6		2.1696	2.1359	2.233[a] 2.179[a] 3.42[b]
Cs_2GeI_6		0.00	0.00	0.00[a] 0.244[a]
Cs_2MnCl_6	spin-up	1.3670	1.4804	–
	spin-down	1.7928	1.6962	–
Cs_2MnI_6	spin-up	0.00	0.00	–
	spin-down	0.8600	1.0527	–

[a]Ref. [18], [b]Ref. [19]

Band structures of Cs_2AX_6 (A = Ge, Mn; X = Cl, I) along the high symmetry directions of the Brillouin zone are depicted in Figs. 4–9. The plots revealed that the investigated double perovskite materials have a direct band gap semiconductor for Cs_2GeCl_6 (GGA-PBE and PBESol) because the conduction band minimum (CBM) and maximum valence band (VBM) lie at the same symmetry point (Γ–Γ). Cs_2GeCl_6 has band gap values of 2.1696 eV and 2.1359 eV for GGA-PBE and PBESol, respectively. As shown in Table II, GGA-PBE has higher band gap values than GGA-PBESol for both Cs_2GeCl_6. The band structure of Cs_2GeI_6 (GGA-PBE and PBESol) shows a zero band gap, indicating that the double perovskite material is metallic. Band gap results obtained for Cs_2AX_6 (A = Ge, Mn; X = Cl, I) are compared with the existing literature in Table II.

The calculated band structure of spin-polarized calculations along the Fermi energy level (E_F) environs for Cs_2MnX_6 (X = Cl, I) are depicted in Figs. 6–9. The results of Cs_2MnCl_6 indicate a semiconductor nature for both spin-up and spin-down, with a band gap of 1.3670 eV and 1.4804 eV for a spin-up for GGA-PBE and PBESol, respectively, while for a spin-down, band gap values are 1.7928 eV and 1.6962 eV for GGA-PBE and PBESol, respectively. Spin-down has higher band gap values than spin-up; additionally, GGA-PBESol has higher band gap values than GGA-PBE in a spin-up, and GGA-PBE has higher band gap values than GGA-PBESol in a spin-down. The calculated band structure for Cs_2MnI_6 spin-up shows zero band gap values for both GGA-PBE and PBESol, indicating that the investigated double perovskite material is metallic, whereas Cs_2MnI_6 spin-down has band gap values of 0.8600 eV and 1.0527 eV for GGA-PBE and PBESol, respectively. In Cs_2MnI_6 spin-down, GGA-PBESol has higher band gap values than GGA-PBE. For Cs_2GeCl_6, the band gap value reduces after replacing Ge with Mn, but the material still retains its semiconductor nature in both spin-up and spin-down, but for Cs_2GeI_6, after introducing Mn, the material remains metal

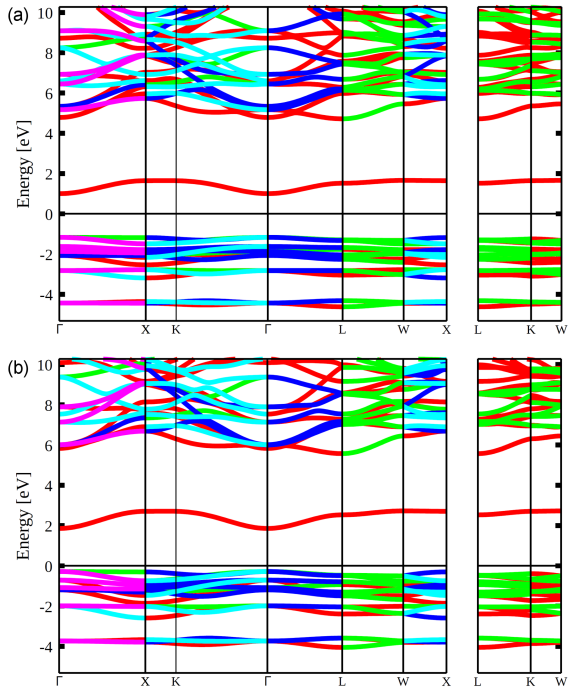

Fig. 4. Band structure plots of (a) Cs_2GeCl_6 (GGA-PBE) and (b) Cs_2GeCl_6 (GGA-PBESol).

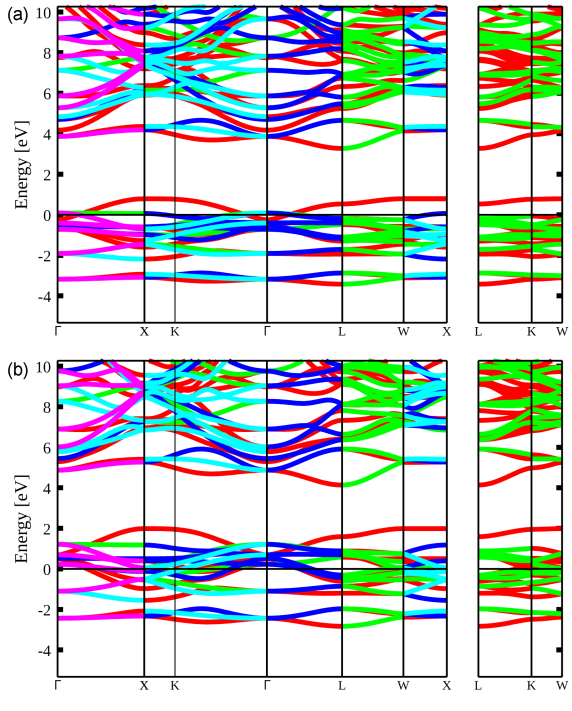

Fig. 5. Band structure plots of (a) Cs_2GeI_6 (GGA-PBE) and (b) Cs_2GeI_6 (GGA-PBESol).

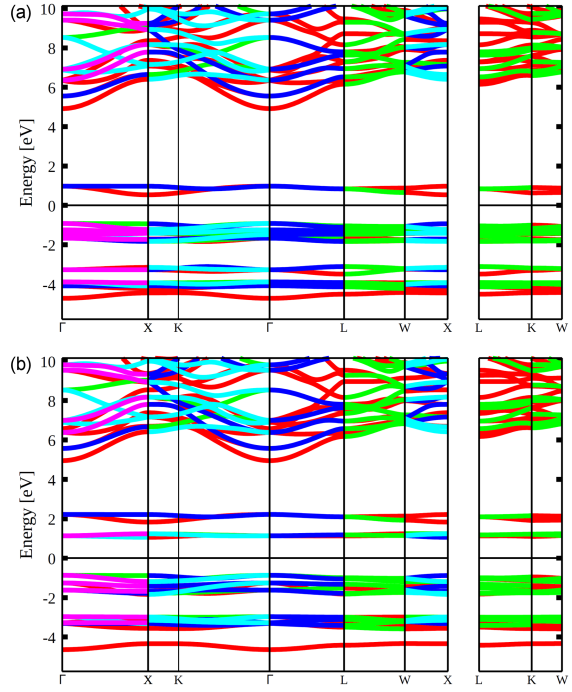

Fig. 6. Band structure plots of Cs_2MnCl_6 using GGA-PBE; (a) spin-up polarization and (b) spin-down polarization.

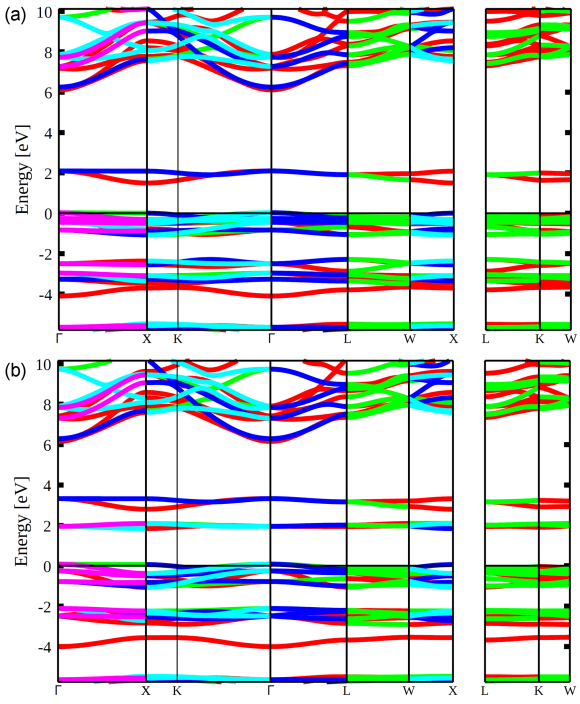

Fig. 7. Band structure plots of Cs_2MnCl_6 using GGA-PBESol; (a) spin-up polarization and (b) spin-down polarization.

with zero band gap in spin-up and has a semiconductor nature in spin-down with a band gap of 0.8600 and 1.0527 eV (GGA-PBE and PBESol, respectively). The occurrence of spin-dependent band gaps, where the band gap differs between different spin orientations (spin-up or spin-down), is evident in specific materials owing to their electronic structure and magnetic characteristics. This phenomenon commonly arises in materials exhibiting spin-polarized electronic states, like

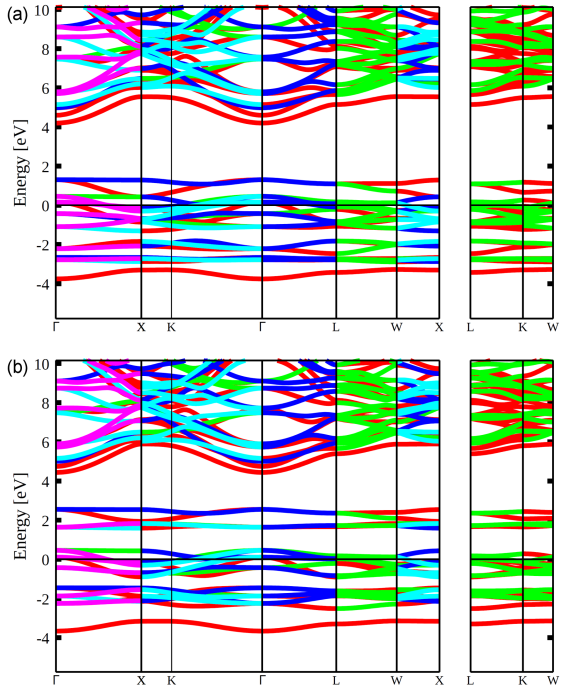

Fig. 8. Band structure plots of Cs_2MnI_6 using GGA-PBE; (a) spin-up polarization and (b) spin-down polarization.

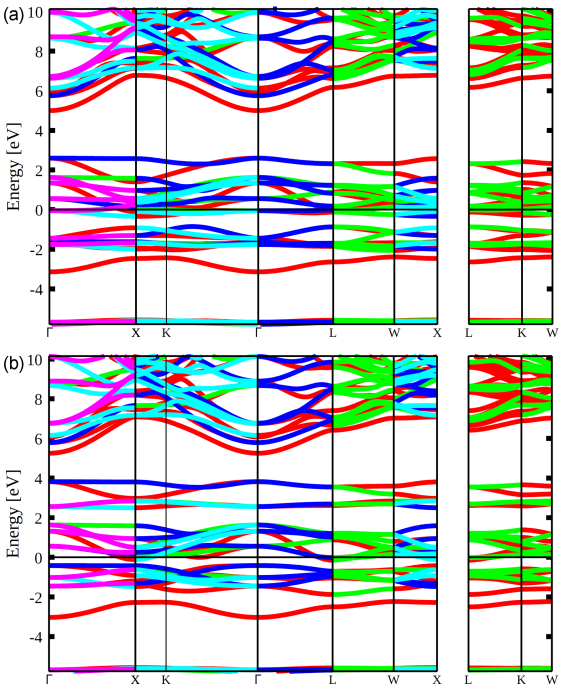

Fig. 9. Band structure plots of Cs_2MnI_6 using GGA-PBESol; (a) spin-up polarization and (b) spin-down polarization.

ferromagnetic or antiferromagnetic materials. Factors contributing to this spin-dependent band gap encompass exchange splitting, magnetic ordering, and spin–orbit coupling effects [43]. The transition

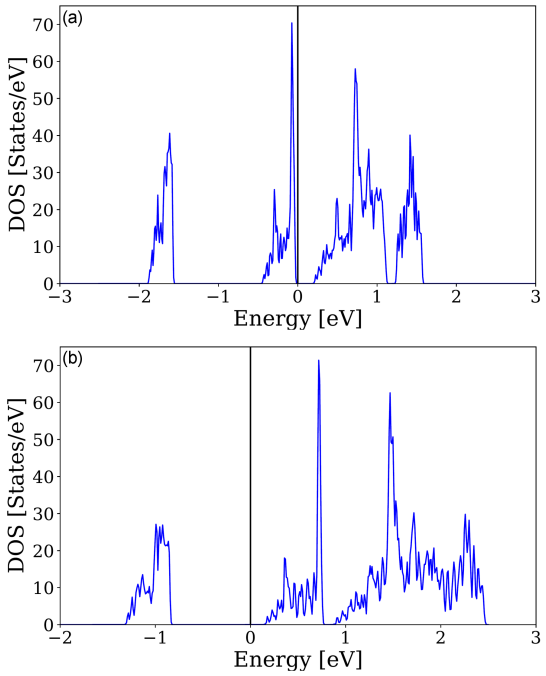

Fig. 10. Density of states of (a) Cs_2GeCl_6 (GGA-PBE) and (b) Cs_2GeCl_6 (GGA-PBESol).

from chloride to iodide anions in double perovskite structures, leading to the observed alteration in electronic behaviour from a semiconductor with a definite band gap to a metallic state, is a result of a combination of factors, including lattice distortion, spin-orbit coupling effects, orbital hybridization [44], and quantum confinement effects [45]. These factors collectively contribute to the transformation of electronic properties.

3.2.2. Density of states

The density of states (DOS) gives useful information regarding the electron transition from the valence to the conduction band while also forecasting the possession of an electronic orbital in the electronic band structure over an energy interval. DOS of a material can easily vary due to the presence of a substitute or dopant element, which results in either improved or degraded device performance [46, 47]. The plots of DOS for Cs_2GeX_6 (X = Cl, I) are shown in Figs. 10–13, where the vertical line represents the Fermi level, which is set to zero energy. From the obtained results, bands for Cs_2GeCl_6 (GGA-PBE and PBESol) do not cross the Fermi energy level (E_F), indicating that the double perovskite material is a semiconductor. A crossing of bands across E_F for Cs_2GeI_6 (GGA-PBE and PBESol) indicates that the double perovskite material has a metallic nature. When Ge is replaced by manganese (Mn) in the investigated double perovskite material Cs_2GeX_6 (X = Cl, I), spin orbits are used in the DOS calculation of Cs_2MnX_6

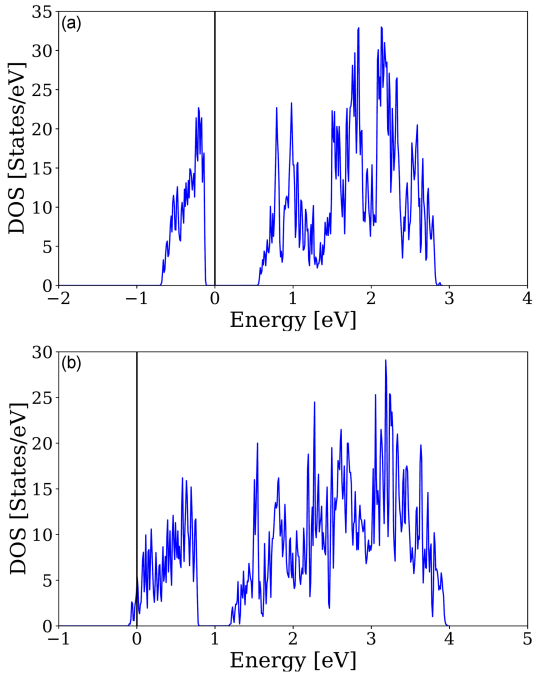

Fig. 11. Density of states of (a) Cs_2GeI_6 (GGA-PBE) and (b) Cs_2GeI_6 (GGA-PBESol).

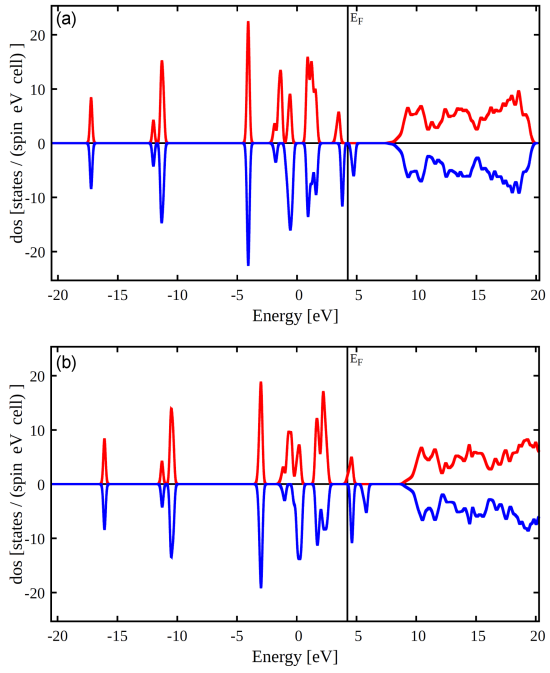

Fig. 12. Spin-polarized density of states for (a) Cs_2MnCl_6 (GGA-PBE) and (b) Cs_2MnCl_6 (GGA-PBESol).

(X = Cl, I). The spin-polarized density of states plots for Cs_2MnX_6 (X = Cl, I) are depicted in Figs. 12 and 13. Note that the bands in Cs_2MnCl_6 (GGA-PBE and PBESol) in both spin-up and spin-down polarization did not cross E_F, indicating that the Cs_2MnCl_6 (GGA-PBE and PBESol) double

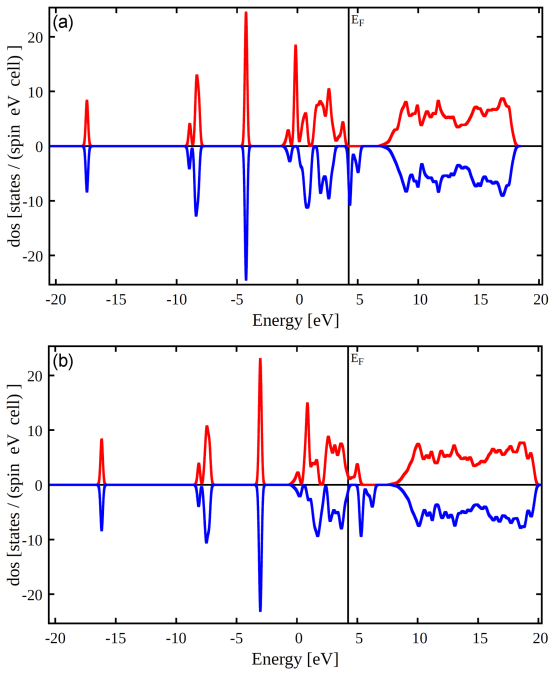

Fig. 13. Spin-polarized density of states for (a) Cs_2MnI_6 (GGA-PBE) and (b) Cs_2MnI_6 (GGA-PBESol).

perovskite material has a semiconductor nature. For Cs_2MnI_6 (GGA-PBE and PBESol), there is a crossing of bands at E_F from the valence band maximum to the conduction band minimum, indicating the metallic nature of the studied double perovskite material, whereas, for spin-down polarization, the bands do not cross E_F, indicating semiconductor nature of the studied double perovskite material. The results support the metallic character for spin-up densities at E_F for Cs_2MnI_6 (GGA-PBE and PBESol) and the semiconductor character for spin-down in Cs_2MnI_6 (GGA-PBE and PBESol). The semi-metallic and metallic character stated in the band structure calculation for Cs_2MnI_6 double perovskite was clearly formed by the substitute element, as seen in Fig. 13. Different electronic properties were observed in spin-up (metallic) and spin-down (semiconductor) in Cs_2MnI_6 double perovskite material, allowing materials to be used for a variety of applications due to the modification in electronic properties. The average intensity of DOS also increases the VBM and CBM near E_F due to the added density of states from Mn.

3.3. Magnetic moments

The magnetic moment is initiated by the exchange division (splitting) of electrons in the Mn-3*d* and Mn-4*d* states. The material's total magnetic moment is the difference between the minority spin state and the majority spin state, which generates magnetic moments [14]. Magnetic properties of the

TABLE III

Magnetic moment of Cs_2MnX_6 (X = Cl, I) studied using GGA-PBE and PBESol.

Material	GGA-PBE [μ_B]	GGA-PBESol [μ_B]
Cs_2MnCl_6	3.0	3.0
Cs_2MnI_6	3.02	3.06

studied double perovskite were investigated due to the advantages, uses, and importance of magnetic materials. Magnetic interaction plays an essential and important role in modern technological appliances [48–50]. Total magnetic moment results for the studied double perovskite material Cs_2MnX_6 (X = Cl, I) using GGA-PBE and PBESol were depicted in Table III. The results show that the total magnetic moment for Cs_2MnCl_6 using GGA-PBE and GGA-PBESol is $3.00\mu_B$ for each exchange–correlation functional, while the total magnetic moment for Cs_2MnI_6 using both GGA-PBE and PBESol is $3.02\mu_B$ and $3.06\mu_B$, respectively, demonstrating the optimal half-metallic property of the studied double perovskite materials [14]. It is worth mentioning that the primary contributor to this total magnetic moment is the transition metal Mn, while elements like Cs, Cl, and I make only a negligible contribution. The presence of magnetic and electronic properties in the Cs_2MnX_6 (X = Cl, I) double perovskite materials shows that they have a magneto-electronic coupling [51]. These magnetic characteristics suggest the compound's potential applications in various fields. This versatility makes it suitable for applications such as computer memories, spintronics, sensors, transformer cores, and microwave components utilizing artificial ferrimagnetic elements for magnetic polarization, among others [48–51].

3.4. Mechanical properties

Investigating the mechanical properties of materials serves a crucial role in understanding both their structural stability and binding characteristics [52, 53]. In the case of cubic systems, only three independent elastic constants (C_{11}, C_{12}, and C_{44}) are required to elucidate mechanical stability, as presented in Table IV (see also [18, 19]). Notably, all positive values of elastic constants adhere to the generalized mechanical stability criteria proposed by Born and Huang [31], as expressed in (1)–(4) [27, 31, 53], which highlights the stability of Cs_2AX_6 (A = Ge, Mn; X = Cl, I) double perovskite material studied using both GGA-PBE and PBESol in its cubic structure.

Employing the Voigt–Reuss–Hill approximations, as outlined in (9) and (10), values of key elastic moduli [28], including the bulk modulus (B), Young's modulus (Y), and shear modulus (G) for Cs_2AX_6 (A = Ge, Mn; X = Cl, I) double perovskite material using both GGA-PBE and PBESol were computed, as presented in Table IV. Young's modulus (Y) is a vital mechanical parameter that reflects a material's stiffness; it is defined as the ratio of tensile stress to tensile strain [29, 48]. A higher value of Young's modulus indicates increased stiffness. Young's modulus (Y) was calculated using (13). The results show that Cs_2MnCl_6 GGA-PBE (17.38) and Cs_2MnCl_6 GGA-PBESol (22.06) have higher values of Y than any other studied double perovskite materials, while Cs_2GeI_6 GGA-PBE (6.10) and Cs_2GeI_6 PBESol (9.11) have lower values of Y, suggesting that Cs_2MnCl_6 exhibits substantial stiffness and is likely to perform as a robust, stiff material.

A good crystal deformation of a material is denoted by its higher bulk modulus (B) values [36]. Bulk moduli for Cs_2AX_6 (A = Ge, Mn; X = Cl, I) (GGA-PBE and PBESol) were computed using (9), and the results are shown in Table IV. One can notice that B values computed using GGA-PBESol are greater than the B values computed using GGA-PBE. Cs_2GeI_6 (GGA-PBESol) have higher B values than other studied double perovskite materials, and this indicates that Cs_2GeI_6 is more rigid and has better crystal deformation than other studied double perovskite materials.

The shear modulus (G), representing the computed plastic deformation characteristics of a material, has been determined using the Voigt–Reuss–Hill approximation [35] as expressed in (10), and its value is reported in Table IV. One can notice that Cs_2MnCl_6 GGA-PBE (7.87 GPa) and Cs_2MnCl_6 GGA-PBESol (9.93 GPa) have higher values of G than any other studied double perovskite materials, while Cs_2GeI_6 GGA-PBE (2.26 GPa) and Cs_2GeI_6 PBESol (3.39 GPa) have lower values of G, indicating that Cs_2MnCl_6 have high level of plastic deformation than other studied double perovskite materials.

Shear anisotropy (A) is used to determine a material's isotropic properties. If $A = 1$, the material is said to be isotropic and can be uniformly deformed along all directions of the material's body, but if the shear anisotropy of a material is less than or greater than unity, the material is an elastic anisotropic material [54]. All the calculated shear anisotropy values for the materials Cs_2AX_6 (A = Ge, Mn; X = Cl, I) are greater than one, implying that they are elastic anisotropic materials.

The Poisson's ratio (ν), as expressed in (14), is a useful quantity for determining important solid-material properties, such as shear stability, nature of inter-atomic force, ductility and brittleness of a material. Materials that are brittle have ν lesser than 0.26, and materials that are ductile have ν greater than 0.26. Cs_2MnCl_6 has ν values of 0.10 and 0.11 for GGA-PBE and PBESol, respectively, which is less than 0.26. This confirms that the material is brittle. In turn, the other studied Cs-based double perovskite materials (Cs_2GeCl_6, Cs_2GeI_6, and Cs_2MnI_6) are ductile because

TABLE IV

Calculated values of mechanical properties using GGA-PBE and PBESol for Cs-based double perovskite materials Cs_2AX_6 (A = Ge, Mn; X = Cl, I).

Material		C_{11} [GPa]	C_{12} [GPa]	C_{44} [GPa]	P_C [GPa]	B [GPa]	G [GPa]	A	Y	ν	R_P	R_F
Cs_2GeCl_6	GGA-PBE	11.65	6.71	4.47	2.24	8.36	3.52	1.81	9.26	0.31	2.37	0.421
	GGA-PBESol	15.05	8.94	6.48	2.46	10.98	4.79	2.12	12.55	0.30	2.29	0.436
	Other works	16.63[a] 39.6[b]	3.77[a] 13.7[b]	6.48[a] 12.2[b]	–	8.16[a] 22.4[b]	6.45[a] 12.5[b]	0.94[b]	15.34[a] 31.6[b]	0.19[a] 0.26[b]	–	–
Cs_2GeI_6	GGA-PBE	8.33	6.66	4.29	2.37	7.21	2.26	5.14	6.10	0.34	3.19	0.313
	GGA-PBESol	13.45	11.73	7.67	4.05	12.30	3.39	8.89	9.18	0.35	3.62	0.276
	Other works	10.60[a]	1.45[a]	6.71[a]	–	4.48[a]	11.77[a]	–	5.54[a]	0.06[a]	–	–
Cs_2MnCl_6	GGA-PBE	16.82	2.54	8.40	−5.86	7.30	7.87	1.13	17.38	0.10	0.92	1.077
	GGA-PBESol	20.70	3.85	11.06	−7.20	9.47	9.93	1.31	22.06	0.11	0.95	1.048
Cs_2MnI_6	GGA-PBE	9.07	6.38	5.13	1.25	7.26	2.99	3.90	7.85	0.31	2.42	0.411
	GGA-PBESol	14.69	10.29	8.92	1.37	11.76	5.12	4.06	13.35	0.30	2.29	0.435

[a]Ref. [18], [b]Ref. [19]

their ν values are greater than 0.26. Cauchy's pressure (P_C), Pugh's ratio (R_P), and Frantsevich's ratio (R_F) can be used to determine the material's brittleness or ductility [19, 47]. If the material's Cauchy pressure is negative, it is brittle; otherwise, it is ductile [55]. Cs_2MnCl_6 has negative P_C values for both GGA-PBE (−5.86) and PBESol (−7.20), respectively, which predicts the material's brittleness. Other studied double perovskite materials (Cs_2GeCl_6, Cs_2GeI_6 and Cs_2MnI_6) are ductile because their P_C values are positive.

Pugh's ratio (R_P) is the ratio of B to G, as expressed in (15). The values of Pugh's ratio show that Cs_2MnCl_6 (using both GGA-PBE and PBESol) is brittle because its R_P is less than 1.75, as confirmed by their ν and P_C values, while Cs_2GeCl_6 (GGA-PBE and PBESol), Cs_2GeI_6 (GGA-PBE and PBESol), and Cs_2MnI_6 (GGA-PBE and PBESol) have $R_P > 1.75$, indicating that they are ductile materials, as confirmed by their ν and P_C results. Frantsevich's ratio (R_F) is the ratio of shear modulus to the bulk modulus and is also known as the inverse of Pugh's ratio, as expressed in (16). Materials is said to be considered brittle if $R_F > 0.571$, otherwise its a ductile [47, 56]. Frantsevich's ratio value of Cs_2MnCl_6 is greater than 0.571 for both GGA-PBE and PBESol, which confirms the brittleness of the material, as do its ν, P_C, and R_P results. Other studied Cs-based double perovskite materials with $R_F < 0.571$, such as Cs_2GeCl_6 (GGA-PBE and PBESol), Cs_2GeI_6 (GGA-PBE and PBESol), and Cs_2MnI_6 (GGA-PBE and PBESol), are ductile materials as confirmed by their ν, P_C, and R_P results.

3.5. Thermoelectric properties

Materials with good thermoelectric properties can be used to convert thermal energy (heat) to electrical energy [36]. The movement of charges for energy transfer produces a heat gradient, which results in a potential difference and a thermoelectric effect [57]. Thermoelectric refrigerators, detectors,

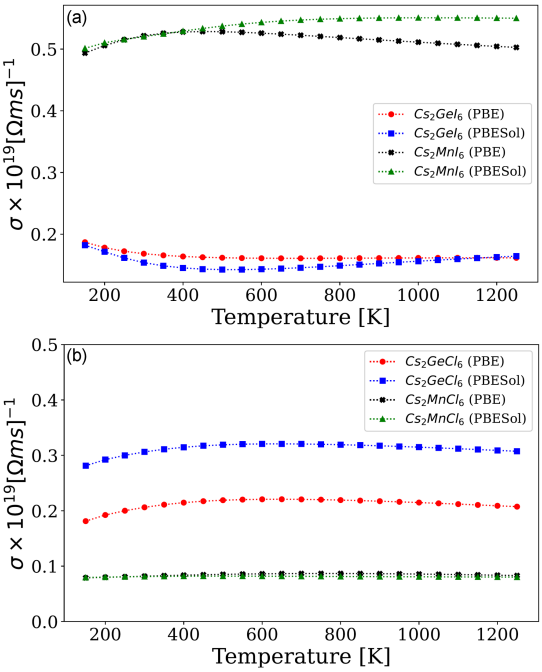

Fig. 14. Electrical conductivity plots computed using GGA-PBE and PBESol of (a) Cs_2GeCl_6 and Cs_2MnCl_6, (b) Cs_2GeI_6 and Cs_2MnI_6.

and cooling systems are some of the practical applications of thermoelectric materials [57]. Due to the low thermal and high electronic conductivity of double perovskite materials, they are widely used for this purpose [36]. Semiconductor materials that have narrow band gap can also be used in TE applications [36]. Sr_3SbN is an antiperovskite with a 1.15 eV bandgap, high thermopower and power factor, but generally, semiconductors have high S values and low thermal conductivity [36, 58]. Most high-performance thermoelectric materials have a bandgap of 0.5–1.5 eV [36, 58]. Materials with higher band gap values have higher S values and materials with lower band gap values have lower S values [36].

3.5.1. Electrical conductivity

Electrical conductivity (σ) plots for Cs-based double perovskite materials Cs_2AX_6 (A = Ge, Mn; X = Cl, I) versus a temperature range of 150–1300 K are depicted in Fig. 14. According to the results, electrical conductivity increases with the increase in temperature for most of the studied Cs-based double perovskite materials. Thermal excitation of electrons into the conduction band leads to this trend for both GGA-PBE and PBESol and for the two studied materials. Electrical conductivity materials reverse the Joule heating effect, due to which they are preferred for TE applications [59]. The plots also show that Cs_2MnCl_6 have higher values of σ at 800 K (0.869×10^{19} $(\Omega\ \mathrm{m\ s})^{-1}$) for GGA-PBESol. The results also show that GGA-PBESol have higher values of σ than GGA-PBE.

3.5.2. Thermal conductivity

The thermoelectric (TE) parameter that combines the effects of lattice (κ_l) and electronic thermal conductivity (κ_e) is known as electronic thermal conductivity (κ_e). BoltzTraP2 calculated only the electronic contribution of thermal conductivity [37]. Due to their lower thermal conductivity, good TE materials have a lower carrier resistance effect, resulting in less carrier collision and heating [36, 60]. The plots of electronic thermal conductivity of studied Cs-based double perovskite materials Cs_2AX_6 (A = Ge, Mn; X = Cl, I) using GGA-PBE and PBESol are shown in Fig. 15. The results show that Cs_2MnI_6 have higher values of κ_e in both GGA-PBE (9.62×10^{14} W/(m K s)) and GGA-PBESol (14.63×10^{14} W/(m K s)), while Cs_2MnCl_6 have lowest values of κ_e in GGA-PBE (1.25×10^{14} W/(m K s)) and GGA-PBESol (1.42×10^{14} W/(m K s)). The ratio of κ_e and σ of the investigated Cs-based double perovskite materials Cs_2AX_6 (A = Ge, Mn; X = Cl, I) is within the range of 10^{-5}, making all the studied materials suitable for thermoelectric applications.

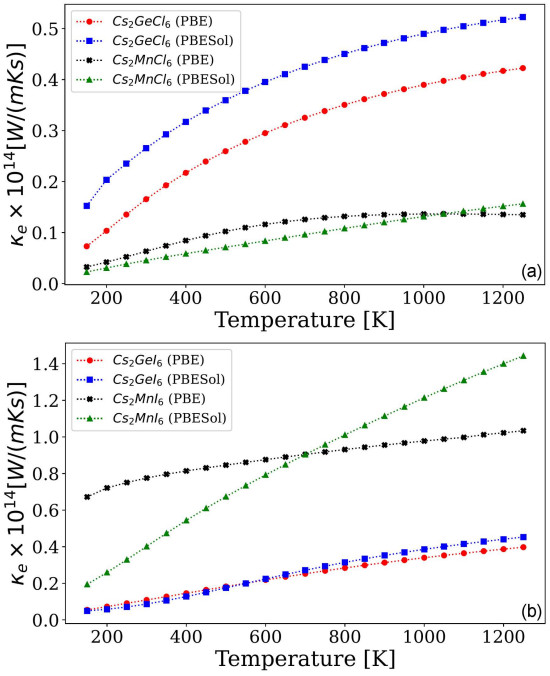

Fig. 15. Thermal conductivity plots computed using GGA-PBE and PBESol of (a) Cs_2GeCl_6 and Cs_2MnCl_6, (b) Cs_2GeI_6 and Cs_2MnI_6.

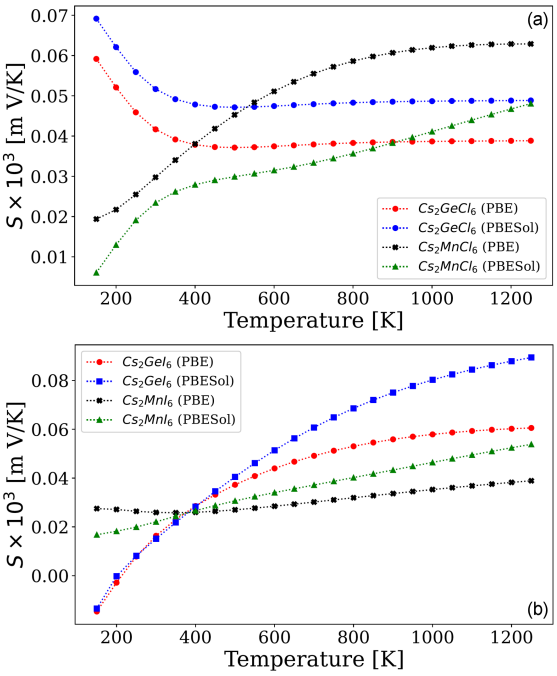

Fig. 16. Seebeck coefficients plots computed using GGA-PBE and PBESol of (a) Cs_2GeCl_6 and Cs_2MnCl_6, (b) Cs_2GeI_6 and Cs_2MnI_6.

3.5.3. Seebeck coefficients (S)

Thermopower, also known as the Seebeck coefficient (S), is a parameter which relates to the electronic structure of a material. According to [36], S is the magnitude of a generated thermo–electric voltage that results from a temperature gradient inside the material. The Seebeck coefficient of a given material can be either negative or positive. If a hole is the dominant charge carrier in a material, the material is said to have positive S, and if an electron is the dominant charge carrier in a material, the material is said to have negative S. Figure 16 shows the plots of Seebeck coefficients of the studied Cs-based double perovskites materials Cs_2AX_6 (A = Ge, Mn; X = Cl, I). This calculated coefficient increases with temperature except for Cs_2GeCl_6, which decreases with an increase in temperature. Among the investigated Cs-based double perovskite materials, Cs_2GeI_6 have higher S values. Due to the positive Seebeck

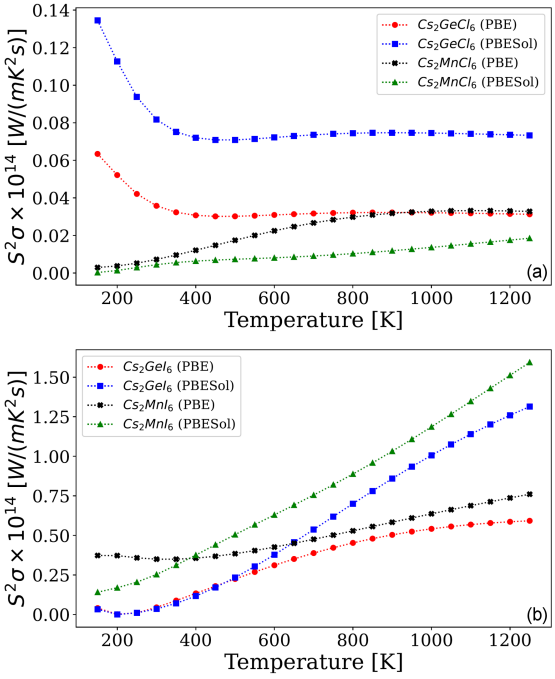

Fig. 17. Power factor plots computed using GGA-PBE and PBESol of (a) Cs_2GeCl_6 and Cs_2MnCl_6, (b) Cs_2GeI_6 and Cs_2MnI_6.

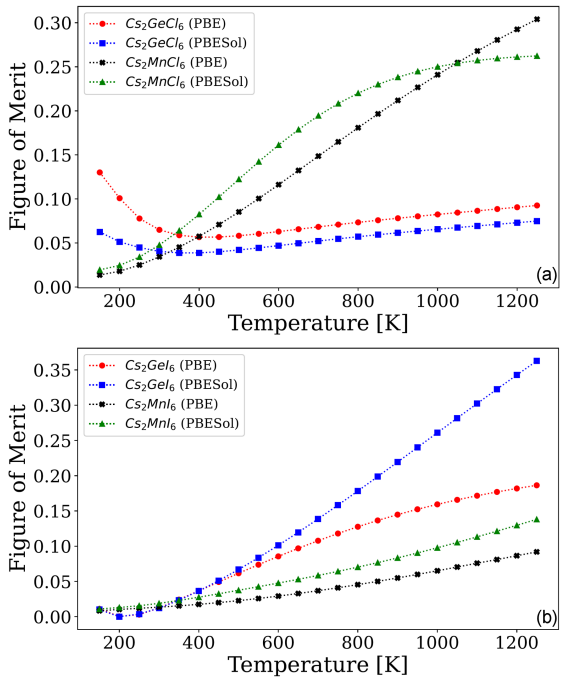

Fig. 18. Figure of merit plots computed using GGA-PBE and PBESol of (a) Cs_2GeCl_6 and Cs_2MnCl_6, (b) Cs_2GeI_6 and Cs_2MnI_6.

coefficient values of Cs_2AX_6 (A = Ge, Mn; X = Cl, I), the investigated Cs-based double perovskite materials exhibit p-type conduction.

3.5.4. Power factor

The power factor (PF) of a material used in thermoelectric applications defines its effective efficiency [38]. Materials with a higher power factor extract heat more effectively [61]. The behaviour of PF of the studied Cs-based double perovskite materials Cs_2AX_6 (A = Ge, Mn; X = Cl, I) was calculated using two different exchange–correlation functionals. The power factor was plotted against temperature for the studied Cs-based double perovskite materials, as shown in Fig. 17. For the studied Cs_2AX_6 (A = Ge, Mn; X = Cl, I) materials, PF increases with an increase in temperature except for Cs_2GeCl_6. Cs_2MnI_6 have higher values of PF in GGA-PBESol (1.65×10^{14} W/(m K^2 s)), followed by Cs_2GeI_6 (1.35×10^{14} W/(m K^2 s)), while Cs_2MnI_6 have low values of PF in both GGA-PBE (0.035×10^{14} W/(m K^2 s)) and GGA-PBESol (0.018×10^{14} W/(m K^2 s)). Materials with higher values of PF are more effective in TE conversion than materials with lower values of PF.

3.5.5. Figure of merit (ZT)

The dimensionless figure of merit (ZT) describes thermoelectric material performance [36, 39]. The quantity ZT refers to a set of material features that have to be enhanced to produce a functional TE generator. To be used in device engineering, a good TE material must have ZT greater than or equal to 1 [57, 62]. Plots of figure of merits ZT versus temperature values ranging from 150 to 1300 K of the studied materials are depicted in Fig. 18. One can notice that Cs_2GeI_6 GGA-PBESol (0.37) have highest value of ZT, followed by Cs_2MnCl_6 GGA-PBE (0.321), while Cs_2MnI_6 GGA-PBESol (0.07) has the lowest value of ZT. The studied Cs-based double perovskite materials have ZT values less than unity, indicating that they have poor ZT values for device engineering.

4. Conclusions

Quantum ESPRESSO code (QE) was used for the calculations of structural, electronic, magnetic, mechanical, and thermoelectric properties of Cs-based double perovskite materials Cs_2AX_6 (A = Ge, Mn; X = Cl, I); interactions between core and valence electrons were described using plane wave method. Norm-conserving pseudopotentials were used to describe electron–ion interactions using GGA-PBE and PBESol. The studied Cs-based double perovskite materials have negative values of enthalpy, which contributes to thermodynamical stability and exothermic reaction. The results indicate that Cs_2GeI_6 and Cs_2MnI_6 have higher values of a [Å], B [GPa], $B^{'}$, and V [Å^3]. Cs_2GeCl_6 and Cs_2MnCl_6 have higher enthalpy [Ry] values than the other Cs-based double perovskite materials studied. The

band structure results show direct band gap semiconductor nature for Cs_2GeCl_6 (GGA-PBE and PBESol) and Cs_2MnCl_6 (GGA-PBE and PBESol) as their bands did not cross E_F; as for Cs_2GeI_6 (GGA-PBE and PBESol) and Cs_2MnI_6 (GGA-PBE and PBESol) their bands crossed E_F from VBM to CBM, indicating that the materials have metallic nature. The calculated total magnetic moment of Cs_2MnCl_6 is $3.0\mu_B$ (for both PBE and PBESol), while for Cs_2MnI_6, it is $3.02\mu_B$ and $3.06\mu_B$, for PBE and PBESol, respectively, demonstrating the optimal half-metallic property of the materials. The presence of magnetic and electronic properties in the material makes it a promising candidate for device applications such as sensors, spintronics, and memory devices, among others. Cauchy's pressure (P_C), Pugh's (R_P), Poisson's (ν), and Frantsevich's ratio (R_F) confirm that Cs_2GeCl_6/I_6 (GGA-PBE and PBESol) and Cs_2MnI_6 (GGA-PBE and PBESol) double perovskite materials are ductile materials, while Cs_2MnCl_6 (GGA-PBE and PBESol) is a brittle material. The thermal-to-electrical ratio of the investigated Cs-based double perovskite materials is of the order of 10^{-5}, making all the studied Cs-based double perovskite materials suitable for TE applications. Positive values of Seebeck coefficients (S) confirmed that the studied materials have p-type conduction.

References

[1] M. Kumar, A. Raj, A. Kumar, A. Anshul, *Opt. Mater.* **111**, 110565 (2021).

[2] M.S.G. Hamed G.T. Mola, *Crit. Rev. Solid State Mater. Sci.* **15**, 1 (2019).

[3] M.I.H. Ansari, A. Qurashi, M.K. Nazeeruddin, *J. Photochem. Photobiol. C Photochem. Rev.* **35**, 1 (2018).

[4] Q. Mahmood, M. Hassan, T.H. Flemban, B. Ul Haq, S. AlFaify, N.A. Kattan, A. Laref, *J. Phys. Chem. Solids 148*, 109665 (2021).

[5] A. Soni, K.C. Bhamu, J. Sahariya, *J. Alloys Compd.* **817**, 152758 (2020).

[6] D. Fabini, *J. Phys. Chem. Lett.* **6**, 3546 (2015).

[7] T. Leijtens, G.E. Eperon, S. Pathak, A. Abate, M.M. Lee, H.J. Snaith, *Nat. Commun.* **4**, 2885 (2013).

[8] S. Li, Z. Zhao, J. Zhao, Z. Zhang, X. Li, X. Zhang, *ACS Appl. Nano Mater.* **3**, 1063 (2020).

[9] X. Liu, Y. Wang, Y. Wang, Y. Zhao, J. Yu, X. Shan, Y. Tong, X. Lian, X. Wan, L. Wang, P. Tian, H.-C. Kuo, *Nanotechnol. Rev.* **11**, 3063 (2022).

[10] K.S. Burch, D. Mandrus, J.G. Park, *Nature* **563**, 47 (2018).

[11] S.A. Khandy, D.C. Gupta, *Mater. Sci. Eng. B* **265**, 114985 (2021).

[12] A. Raj, M. Kumar, D. Mishra, A. Anshul, *Opt. Mater.* **101**, 109773 (2020).

[13] S.A. Khandy, D.C. Gupta, *J. Magn. Magn. Mater.* **458**, 176 (2018).

[14] M. Kumar, A. Raj, A. Kumar, S. Sharma, H. Bherwani, A. Gupta, A. Anshul, *Opt. Int. J. Light Electron Opt.* **242**, 166746 (2021).

[15] A. Anshul, M. Kumar, A. Raj, *Optik* **212**, 164749 (2020).

[16] K.F. Wang, J.M. Liu, Z.F. Ren, *Adv. Phys.* **58**, 321 (2009).

[17] A. Ilyas, S.A. Khan, K. Liaqat, T. Usman, *Opt. Int. J. Light Electron Opt.* **244**, 167536 (2021).

[18] X. Diao, Y. Diao, Y. Tang, G. Zhao, Y. Gu, Q. Xie, Y. Shi, L. Zhang, P. Zhu, *Sci. Rep.* **12**, 12633 (2022).

[19] Q. Mahmood, T. Ghrib, A. Rached, A. Laref, M.A. Kamran, *Mater. Sci. Semicond. Proces.* **112**, 105009 (2020).

[20] Y. Cai, W. Xie, H. Ding, Y. Chen, T. Krishnamoorthy, L.H. Wong, N. Mathews, S.G. Mhaisalkar, M. Sherburne, M. Asta arXiv:1706.08674v1 (2017).

[21] P. Giannozzi, S. Baroni, N. Bonini et al., *J. Phys. Condens. Matter* **21**, 395502 (2009).

[22] P. Giannozzi, O. Andreussi, T. Brumme et al., *J. Phys. Condens. Matter* **29**, 465901 (2017).

[23] J.P. Perdew, K. Burke, M. Ernzerhof, *Phys. Rev. Lett.* **77**, 3865 (1996).

[24] J.D. Pack, H.J. Monkhorst, *Phys. Rev. B Condens. Matter Mater. Phys.* **16**, 1748 (1977).

[25] C.G. Broyden, *IMA J. Appl. Math.* **6**, 76 (1970).

[26] C.G. Broyden, *IMA J. Appl. Math.* **6**, 222 (1970).

[27] A.A. Sholagberu, W.A. Yahya, A.A. Adewale, *Phys. Scr.* **97**, 085824 (2022).

[28] S.A. Dar, R. Sharma, V. Srivastava, U.K. Sakalle, *RSC Adv.* **9**, 9522 (2019).

[29] S.A. Dar, V. Srivastava, U. Kumar, U.K. Sakalle, A. Vanshree, V. Parey, *Eur. Phys. J. Plus* **133**, 1 (2018).

[30] G.V. Sin'ko, N.A. Smirnov, *J. Phys. Condens. Matter* **14**, 6989 (2002).

[31] M. Born, K. Huang, M. Lax, *Am. J. Phys.* **23**, 474 (1955).

[32] D.H. Chung, W.R. Buessem, *J. Appl. Phys.* **38**, 2535 (1967).

[33] W. Voigt, *Lehrbuch der Kristallphysik*, Spring Fachmedien Wiesbaden, 1928, p. 980 (reproduced 1966).

[34] A. Reuss, *Z. Angew. Math. Mech.* **9**, 49 (1929).

[35] R. Hill, *Proc. Phys. Soc.* **65**, 349 (1952).

[36] W.A. Yahya, A.A. Yahaya, A.A. Adewale, A.A. Sholagberu, N.K. Olasunkanmi, *J. Nig. Soc. Phys. Sci.* **5**, 1418 (2023).

[37] G.K.H. Madsen, J. Carrete, M.J. Verstraete, *Comput. Phys. Commun.* **231**, 140 (2018).

[38] V. Kumar, M. Kumar, M. Singh, *Mater. Today Proc.* **62**, 3811 (2022).

[39] G. Woolman, Ph.D. thesis, The University of Edinburgh, 2021.

[40] D. Behera S.K. Mukherjee, *Chemistry* **4**, 1 (2022).

[41] M. Waqas, *Sci. Inquiry Rev.* **4**, 01 (2020).

[42] S. Zhao, K. Yamamoto, S. Iikubo, S. Hayase, T. Ma, *J. Phys. Chem. Solids* **117**, 117 (2018).

[43] P. Fulde, *Electron Correlations in Molecules and Solids*, Vol. 100, Springer Science & Business Media, 2012.

[44] D. Saparov D.B. Mitzi, *Chem. Rev.* **116**, 4558 (2016).

[45] D.B. Mitzi, in: *Progress in Inorganic Chemistry*, Vol. 48, Ed. K.D. Karlin, John Wiley & Sons 1999 p. 1.

[46] J.W. Haus, *Fundamentals and Applications of Nanophotonics*, 1st ed., Woodhead Publishing, 2016.

[47] A.A. Adewale, A. Chik, T. Adam, T.M. Joshua, M.O. Durowoju, *Mater. Today Commun.* **27**, 102077 (2021).

[48] A.B. Siad, M. Baira, F.Z. Dahou, K. Bettir, M.E. Monir, *J. Solid State Chem.* **302**, 122362 (2021).

[49] M.D.I. Bhuyan, S. Das, M.A. Basith, *J. Alloys Compd.* **878**, 160389 (2021).

[50] G.A.M. Mersal, H. Alkhaldi, G.M. Mustafa, Q. Mahmood, A. Mera, S. Bouzgarrou, A. Badawi, A.A. Shaltout, J. Boman, M.A. Amin, *J. Mater. Res. Technol.* **18**, 2831 (2022).

[51] S. Haida, W. Benstaalia, A. Abbada, B. Bouadjemia, S. Bentatab, Z. Aziza, *Mater. Sci. Eng. B* **245**, 68 (2019).

[52] B. Holm, R. Ahuja, Y. Yourdshahyan, B. Johansson, B.I. Lundqvist, *Phys. Rev. B* **59**, 12777 (1999).

[53] F. Mouhat F.-X. Coudert, *Phys. Rev. B* **90**, 224104 (2014).

[54] J.N. Nye, *Physical Properties of Crystals Their Representation by Tensors and Matrices*, Oxford University Press, 1985.

[55] D.G. Pettifor, *Mater. Sci. Technol.* **8**, 345 (1992).

[56] I.N. Frantsevich, F.F. Voronov, S.A. Bokuta, *Elastic Constants and Elastic Moduli of Metals and Insulators — A Handbook*, Vol. 7, Naukova Dumka, Kiev 1983.

[57] A.H. Reshak, *Mater. Sci. Semicond. Proces.* **148**, 106850 (2022).

[58] L.D. Zhao, S.H. Lo, Y. Zhang, H. Sun, G. Tan, C. Uher, C. Wolverton, V.P. Dravid, M.G. Kanatzidis, *Sci. Nat.* **508**, 373 (2014).

[59] R. Ullah, A.H. Reshak, M.A. Ali, *Int. J. Energy Res.* **45**, 8711 (2021).

[60] M. Hassan, I. Arshad, Q. Mahmood, *Semicond. Sci. Technol.* **32**, 115002 (2017).

[61] M. Saeed, I. Ul-Haq, A.S. Saleemi, S. Ur-Rehman, B. Ul-Haq, A.R. Chaudhry, I. Khan, *J. Phys. Chem. Solids* **160**, 110302 (2022).

[62] T. Takeuchi, *Mater. Trans.* **50**, 2359 (2009).